

Technical Note: A software framework for calculating compositionally dependent *in situ* ^{14}C production rates

Alexandria J. Koester¹, Nathaniel A. Lifton^{1,2}

¹Department of Earth, Atmospheric, and Planetary Sciences, Purdue University, West Lafayette, IN 47907, USA

5 ²Department of Physics and Astronomy, Purdue University, West Lafayette, IN 47907, USA

Correspondence to: Alexandria J. Koester (koestea@purdue.edu)

Abstract

Over the last 30 years, *in situ* cosmogenic nuclides (CNs) have revolutionized surficial process and Quaternary geologic
10 studies. Commonly measured CNs extracted from the common mineral quartz have long half-lives (e.g., ^{10}Be , ^{26}Al), and have
been applied over timescales from a few hundred years to millions of years. However, their long half-lives also render them
largely insensitive to complex histories of burial and exposure less than ca. 100 ky. On the other hand, *in situ* cosmogenic ^{14}C (*in*
situ ^{14}C) is also produced in quartz, yet its 5.7 ky half-life renders it very sensitive to complex exposure histories during the last
~25 ka – a particularly unique and powerful tool when analyzed in concert with long-lived nuclides. *In situ* ^{14}C measurements
15 are currently limited to relatively coarse-grained (typically sand-sized or larger, crushed/sieved to sand) quartz-bearing rock
types, but while such rocks are common, they are not ubiquitous. The ability to extract and interpret *in situ* ^{14}C from quartz-poor
and fine-grained rocks would thus open its unique applications to a broader array of landscape elements and environments.

As a first step toward this goal, a robust means of interpreting *in situ* ^{14}C concentrations derived from rocks and minerals
spanning wider compositional and textural ranges will be crucial. We have thus developed a MATLAB[®]-based software
20 framework to quantify spallogenic production of *in situ* ^{14}C from a broad range of silicate rock and mineral compositions,
including rocks too fine-grained to achieve pure quartz separates. As expected from prior work, production from oxygen
dominates the overall *in situ* ^{14}C signal, accounting for >90% of production for common silicate minerals and six different rock
types at sea-level and high latitudes (SLHL). This work confirms that Si, Al, and Mg are important targets, but also predicts
greater production from Na than from those elements. The compositionally dependent production rates for rock and mineral
25 compositions investigated here are typically lower than that of quartz, although that predicted for albite is comparable to quartz,
reflecting the significance of production from Na. Predicted production rates drop as compositions become more mafic
(particularly Fe-rich). This framework should thus be a useful tool in efforts to broaden the utility of *in situ* ^{14}C to quartz-poor
and fine-grained rock types, but future improvements in measured and modelled excitation functions would be beneficial.

1 Introduction

30 Rare nuclides produced *in situ* in minerals near the Earth's surface by cosmic-ray bombardment (*in situ* cosmogenic nuclides
or CNs) have revolutionized studies of geomorphology and Quaternary geology. CNs build predictably over time in an exposed
surface through nucleon spallation and muon reactions (e.g., Gosse and Phillips, 2001). As such, the time at which geomorphic
surfaces formed by glacial, fluvial, or marine activity often can be constrained with CNs, an application known as surface
exposure dating. In addition, CNs can be used to constrain rates of surficial processes with appropriate interpretive models.
35 These applications rely on measuring the concentrations (atoms g^{-1}) of CNs in a sample and calculating an exposure age or

erosion rate based on the production rate (atoms $\text{g}^{-1} \text{y}^{-1}$). The most-commonly measured CNs, ^{10}Be and ^{26}Al ($t_{1/2}$ 1.39 My - Korschinek et al. (2010); Chmeleff et al. (2010); and $t_{1/2}$ 0.705 My - Nishiizumi et al. (2004), respectively), are typically extracted from quartz, due to its simple composition and corresponding resistance to weathering under a wide range of environmental conditions. Their long half-lives make these nuclides useful in dating surfaces that have been exposed up to millions of years. However, their half-lives also render their concentrations insensitive to periods of burial and re-exposure of less than ca. 100 ky – this can lead to problems with exposure dating due to nuclide inventories remaining from prior periods of exposure.

In situ cosmogenic ^{14}C (*in situ* ^{14}C) is also produced in quartz, but its 5.7 ky half-life limits its utility for simple exposure dating because its concentration reaches secular equilibrium between production and decay after 25-30 ky of continuous exposure. However, its rapid decay also makes it sensitive to complex periods of burial and exposure since ca. 25-30 ka (e.g., Briner et al., 2014). In addition, its short half-life means measured concentrations are sensitive only to very rapid erosion rates (e.g., Gosse and Phillips, 2001; von Blanckenburg et al., 2005; Hippe et al., 2017; Hippe et al., 2021), making many eroding landscape elements good targets for *in situ* ^{14}C studies. *In situ* ^{14}C is thus emerging as a powerful addition to the CN toolkit.

Several techniques for extracting *in situ* ^{14}C from sand-sized quartz grains have been established (Lifton et al., 2001; Lifton et al., 2015; Goehring et al., 2019; Hippe et al., 2013; Lupker et al., 2019; Fülöp et al., 2019), but while coarse-grained quartz is common, it is not ubiquitous. Landscapes dominated by mafic or intermediate lithologies generally lack quartz, and fine-grained lithologies can limit the efficacy of quartz purification techniques thus applying *in situ* ^{14}C to such rock types is currently problematic. However, the ability to extract and interpret *in situ* ^{14}C concentrations reliably from quartz-poor and fine-grained lithologies would significantly broaden its applications to additional landscapes and enable pairing with additional nuclides such as ^{36}Cl . Indeed, early studies of *in situ* ^{14}C in terrestrial rocks utilized whole-rock samples (e.g., Jull et al., 1992; 1994), until procedural difficulties shifted the focus to the simpler quartz production and extraction systematics (Lifton, 1997; Lifton et al., 2001).

As a first step in expanding the range of available sample targets, we have developed a software framework that estimates the production of *in situ* ^{14}C from major elements found in typical rocks and potential mineral separates. We modified the MATLAB® code from Lifton et al. (2014) to calculate compositionally dependent, site-specific production rates using nuclide-specific scaling, major-element oxide compositions, and measured and modelled nucleon excitation functions, referenced to geologically calibrated *in situ* ^{14}C spallogenic production rates in quartz. Anticipating that appropriate extraction and CO_2 purification procedures can be developed, this new framework thus provides a critical first step for potential future applications incorporating quartz-poor or fine-grained samples.

2 Constraining compositionally dependent *in situ* ^{14}C production rates

2.1 Geologic and experimental production rate calibrations

In situ CN applications require accurate estimates of the rate at which a given nuclide of interest is produced in the target mineral or rock. This is typically achieved by calibrating the production rate with CN measurements in samples from one or more sites with 1) an independently well-constrained exposure history (e.g., Borchers et al., 2016; Phillips et al., 2016; Lifton et al., 2015a), or for radionuclides only, with 2) demonstrable surface stability such that measured CN concentrations can be inferred to have reached a secular equilibrium between production and decay, at which point the concentration is only a function

of time-integrated production rate and the decay constant (e.g., Jull et al., 1992; Borchers et al., 2016). Production rates can also be calibrated experimentally by exposing high-purity, low background targets to the secondary cosmic-ray flux at given sites for a known duration under well-constrained conditions (e.g., Nishiizumi et al., 1996; Brown et al., 2000; Vermeesch et al., 2009).

75 Since production rates cannot be calibrated at every place on Earth, these site-specific estimates are typically scaled to other sites of interest using an appropriate scaling framework that accounts for spatial and temporal variations in the secondary cosmic-ray flux, arising from fluctuations in the geomagnetic field (parameterized by effective vertical cutoff rigidity, R_C , in GV), atmospheric depth (X , in g cm^{-2}), and solar modulation (described by the parameter Φ , in MeV) (e.g., Lifton et al., 2014). Such scaling frameworks are typically referenced to conditions corresponding to sea-level and high geomagnetic latitude
80 (SLHL).

Geologic calibrations are generally preferable for minerals with specific compositions since samples from sites with independently well-constrained exposure histories should incorporate natural geologic variability relevant over geologic time spans. Such calibrations for *in situ* ^{14}C have focused on quartz to date, given its simple chemistry and weathering resistance, as noted above (e.g., Borchers et al., 2016; Phillips et al., 2016; Lifton et al., 2015a; Schimmelpfennig et al., 2012; Young et al.,
85 2014), yet variable compositions require more complicated consideration of the compositional dependence of CN production (e.g., ^{36}Cl ; Marrero et al., 2016a). It is often useful in such cases to utilize theoretical production rate estimates based on integrals of the differential cosmic-ray flux and the relationship between reaction probability and incident particle energy.

2.2 Theoretical production rate estimates

The probability that a given nuclear reaction will occur at a given kinetic energy E of an incident particle is described by the
90 reaction cross-section (σ), in units of barns ($1 \text{ barn} = 10^{-24} \text{ cm}^2$). With the advent of accelerator mass spectrometry (AMS), cross-section measurements for reactions producing CNs have become relatively common, and knowledge of the variation of σ as a function of E for those reactions (known as an excitation function) are continuing to improve (e.g., Reedy, 2013). Proton-induced reactions are simpler to measure than those induced by neutrons because it is easier to accelerate protons into a mono-energetic beam. Mono-energetic (or quasi-mono-energetic) neutron reaction cross-sections are more difficult to obtain, however,
95 and thus are often estimated from analogous proton cross-sections (Reedy, 2013).

Measured or modelled excitation functions can then be used to estimate theoretical production rates for a CN of interest using Eq. (1) below (e.g., Masarik and Beer, 2009),

$$P_j(X, R_C, \Phi) = \sum_i ND_i \sum_k \int_0^\infty \sigma_{ijk}(E_k) J_k(E_k, X, R_C, \Phi) dE_k \quad (1)$$

where ND_i is the target number density, or number of atoms of the target element i per gram of sample material (atoms g^{-1}),
100 $\sigma_{ijk}(E_k)$ is the cross-section for the production of nuclide j (cm^2) by particles of type k with energy E_k (MeV), and $J_k(E_k, X, R_C, \Phi)$ is the differential flux of atmospheric cosmic-ray particles ($\text{cm}^{-2} \text{ y}^{-1} \text{ MeV}^{-1}$) of type k with energy E_k at a location and time specified by X , R_C , and Φ .

The production of *in situ* ^{14}C in silicates is dominantly from spallation of O, and theoretical simulations suggest minor spallogenic production from Mg, Al, and Si (Masarik and Reedy, 1995; Masarik, 2002). Production of *in situ* ^{14}C from muons
105 also occurs, either via slow negative muon capture or by fast muon interactions (Heisinger et al., 2002a,b; Lupker et al., 2015; Balco, 2017). The muogenic component of *in situ* ^{14}C production in surficial quartz at SLHL is significant – on the order of 20% of total production (e.g., Lupker et al., 2015; Balco, 2017). However muogenic production of *in situ* ^{14}C has only been estimated

experimentally from ^{16}O (Heisinger et al., 2002a,b). Further work is needed in this area to better understand production from other muogenic reactions. We therefore focus on the dominant spallogenic pathways for the purposes of this initial study.

110 3 Methods

3.1 Software framework

Our MATLAB[®]-based compositionally dependent *in situ* ^{14}C production rate software framework builds on the LSDn nuclide-dependent scaling formulation of Lifton et al. (2014), which uses the PARMA analytical approximations to Monte Carlo calculations of atmospheric differential flux spectra of neutrons, protons, and muons as a function of X , R_C , and Φ (Sato et al., 115 2006; 2008). We also incorporate the time-dependent gridded R_C (global grids of cutoff rigidity) and dipolar R_{CD} (geocentric dipolar cutoff rigidity) models of Lifton et al. (2016), based on the SHA.DIF.14k paleomagnetic model (Pavón-Carrasco et al., 2014). This work accounts for effects of variable sample compositions on *in situ* ^{14}C production by incorporating relevant reaction excitation functions and number densities for elements in the standard suite of major-element oxide compositions. Output from this new framework should complement current web-based cosmogenic nuclide calculators incorporating the LSDn 120 scaling framework and *in situ* ^{14}C , including version 3 of the University of Washington cosmogenic-nuclide calculators (herein UWv3: hess.ess.washington.edu) (Balco et al., 2008) and the Cosmic-Ray-produced NUclide Systematics on Earth project (CRONUS-Earth) calculator (CRONUSCalc; <http://cronus.cosmogenicnuclides.rocks/>; Marrero et al., 2016b).

Reaction excitation functions for neutrons and protons were compiled from Reedy (2007; 2013) and the JENDL/HE-2007 database (Fukahori et al., 2002; Watanabe et al., 2011) found in the online Evaluated Nuclear Data File (ENDF, [https://www- 125 nds.iaea.org/exfor/endl.htm](https://www-nds.iaea.org/exfor/endl.htm), accessed April 2020; Brown et al., 2018) for each of the major elements included in typical elemental oxide analyses. We consider empirical excitation functions to be generally more reliable than those derived from nuclear reaction models, and thus use empirical functions if available. Five neutron and proton excitation functions are based on measurements from Reedy (2007, 2013) of elements at natural isotopic abundances (O, Mg, Al, Si, Fe), while we used modelled neutron and proton reaction excitation functions from JENDL/HE-2007 for the most abundant isotopes of the remaining 130 elements considered (^{23}Na , ^{31}P , ^{39}K , ^{40}Ca , ^{48}Ti , ^{55}Mn). Apart from the measured excitation function for *in situ* ^{14}C production by neutron spallation from oxygen (Reedy, 2013), it is important to note that most of the Reedy (2007, 2013) neutron excitation functions are not directly measured but instead are derived from measured proton excitation functions. We utilized the JENDL/HE-2007 database because the relevant excitation functions extended to a maximum energy of 3 GeV, close to the maximum 10 GeV energy considered by Sato et al. (2006, 2008); a version of that nuclear data library was also utilized by those 135 studies. The exceptions were the excitation functions for ^{31}P , extending only to 0.2 GeV. Each excitation function was interpolated into logarithmic energy bins from 1 MeV to 200 GeV for both neutron ($\text{XX}(\text{n},\text{x})^{14}\text{C}$) and proton ($\text{XX}(\text{p},\text{x})^{14}\text{C}$) reactions, where XX is the target nuclide (Fig. 1). The cross-section at the highest measured or modelled energy reported for each excitation function is assumed to be constant beyond that energy up to 200 GeV, the maximum energy we consider.

We incorporate sample compositions using common major elemental oxide analyses (e.g., from X-Ray Fluorescence (XRF) 140 measurements) to calculate ND for each element considered in Eq. 1. The ND value for each target element in a sample is then calculated per Eq. (2), for input to Eq. 1:

$$ND = \frac{E_{Fr} * E_{Ox} * N_A}{100 * A_m}, \quad (2)$$

where E_{Fr} is the elemental fraction in each oxide (formula mass of each element in its oxide divided by the total formula mass of the oxide (e.g., Mg/MgO or 2Al/Al₂O₃)), E_{Ox} is the measured major elemental oxide weight percent input by the user, N_A is
145 Avogadro's number ($6.02214076 \times 10^{23}$ atoms mol⁻¹) and A_m is the molar mass of the element in g. This approach works for any silicate major elemental oxide composition input by the user.

3.2 Predicted compositionally dependent production rates

Theoretical compositionally dependent site-specific *in situ* ¹⁴C production rates are reported relative to the SLHL *in situ* ¹⁴C
150 global production rate in quartz, geologically calibrated as part of the CRONUS-Earth project (e.g., Borchers et al, 2016; Phillips et al., 2016) and supplemented with two subsequent production rate calibration datasets (Schimmelpfennig et al., 2012; Young et al., 2014), using the LSDn scaling framework (Lifton et al., 2014, Lifton 2016) (Supplemental Information, Table S1). All *in situ* ¹⁴C measurements in these studies were recalculated following Hippe and Lifton (2014). SLHL estimates are referenced to the year 2010 (Lifton et al., 2014; Lifton, 2016) assuming an atmospheric pressure of 1013.25 hPa (converted to atmospheric depth, g cm⁻²), an R_c value of 0 GV, a Φ_{2010} value of 624.5718 MV, and a fractional water content value, ' w ', of 0.066 (Sato et al.,
155 2006; Phillips et al. 2016). We recalibrated the *in situ* ¹⁴C spallogenic production rate at SLHL in quartz from the studies above by first calculating the unweighted mean and standard deviation of replicate analyses of samples at each site (to avoid biasing the results toward sites with more analyses). Best-fitting SLHL production rate estimates for each site were determined using a χ^2 minimization procedure. The unweighted mean and standard deviation of all sites were then calculated from the site-specific SLHL production rate estimates, yielding global SLHL values for quartz of 13.5 ± 0.9 atoms g⁻¹ y⁻¹ and 13.7 ± 1.2 atoms g⁻¹ y⁻¹
160 for the gridded R_C and geocentric dipolar R_{CD} records of Lifton (2016), respectively, as noted above. The latter is comparable to the calibrated value generated by the UWv3 calculator from the same dataset (Table S1). In the following discussion we focus on the gridded R_C value (referenced below as P_{Qcal}), as it provides a somewhat better fit to the global calibration dataset. Corresponding geocentric dipolar values are included in Table S2.

For comparison, the purely theoretical *in situ* ¹⁴C production rate by nucleon spallation predicted at SLHL in quartz using
165 Eq. 1 is 15.8 atoms g⁻¹ y⁻¹ (P_{Qref}). This discrepancy with the calibrated value likely reflects uncertainties in both the excitation functions and the nucleon fluxes considered (Reedy, 2013; Sato et al., 2006; Sato et al., 2008). Giving more credence to the geologically calibrated quartz values, we account for this discrepancy similarly to Lifton et al. (2014), deriving a compositionally dependent site-specific production rate (P_{CD}) by normalizing the predicted compositionally dependent production rate at the site of interest (P_{CDpred}) by the ratio of P_{Qcal} to P_{Qref} , per Eq. 3. Another way to think of this is that the ratio
170 of P_{CDpred} to P_{Qref} is the compositionally dependent scaling factor, multiplied by the geologically calibrated production rate in quartz, P_{Qcal} .

$$P_{CD} = P_{Qcal} \frac{P_{CDpred}}{P_{Qref}} \text{ atoms g}^{-1} \text{ y}^{-1} \quad (3)$$

We compare P_{CD} values at SLHL to P_{Qcal} for compositions reflecting both individual minerals (Barthelmy, 2014; Morimoto, 1988) (i.e., mineral separates) and a broad range of silicate rock types (Parker, 1967; Fabryka-Martin, 1988) (i.e., whole-rock
175 analyses) (Table 1). A pure calcite composition (CaCO₃) is assumed for limestone and MgCa(CO₃)₂ is assumed for dolomite. Spallation production in this case is only possible from Ca and O, although we included the O number density contribution from CO₂ in the software framework. Thermal neutron production of *in situ* ¹⁴C from ¹²C or ¹³C is expected to be negligible and is not considered here (e.g., Wright et al., 2019).

4 Results and Discussion

4.1 Predicted modern production rates for silicate minerals and rock types

Predicted SLHL modern (i.e., 2010) spallogenic production rates for *in situ* ^{14}C in the silicates considered here are generally lower than that from pure quartz (Fig. 3; Table 2), but spallation production from O dominates throughout the compositional range we explored (Table 3). As expected from reaction systematics, ^{14}C production rates tend to decline rapidly with progressively increasing atomic mass of the target nuclide (Fig. 3). Interestingly, the production rate predicted for albite using the excitation functions from JENDL/HE-2007 for spallation reactions on ^{23}Na is comparable to that of quartz. We note that the JENDL/HE-2007 model $^{23}\text{Na}(\text{n},\text{x})^{14}\text{C}$ excitation function exhibits a broad peak between ca. 30-350 MeV with cross-sections comparable to that of the empirical $\text{O}(\text{n},\text{x})^{14}\text{C}$ excitation function of Reedy (2013) (Fig. 1), suggesting similar production magnitudes for the two reactions. To our knowledge, no comparable empirical excitation functions for the $^{23}\text{Na}(\text{n},\text{x})^{14}\text{C}$ or $^{23}\text{Na}(\text{p},\text{x})^{14}\text{C}$ reactions have been published to date, making the model reactions difficult to validate. Predicted production rates for Mg-rich silicates such as forsterite and enstatite are ca. 7-10% lower than in quartz, while Al-rich minerals such as Ca- and K-feldspars yield production rates 12-13% below quartz. Ca-rich wollastonite exhibits less than 1% of its total ^{14}C production from Ca, yielding a production rate more than 20% below that of quartz, while Fe-rich minerals such as ferrosilite and fayalite suggest SLHL production rates ca. 32% and 41% less than quartz, respectively. Predicted production rates for two carbonate minerals considered, calcite and dolomite, are 12% and 3% less than quartz, respectively.

The P_{CD} values for selected rock types (ultramafic, basalt, high-Ca granite, low-Ca granite, and granodiorite; Fabryka-Martin, 1988) follow a similar pattern to the individual minerals, with total production rates less than that of quartz but with less overall variation (Fig. 3; Table 2). Predicted whole-rock production rates tend to increase with decreasing Fe and Mg content, with P_{CD} values ranging from nearly 15% less than quartz for ultramafic compositions to ca. 5-7% below that of quartz for more felsic compositions. As with the idealized mineral compositions, spallation from O dominates *in situ* ^{14}C production (>90% for all compositions considered), with lesser production from Si, Al, Na, and Mg. Only minor production contributions from Ca and Fe are predicted (typically <1%).

4.2 Assessing uncertainty in predicted compositionally dependent production rates

There are three main sources of uncertainty in our predicted production rates, associated with the particle spectra, the geologic production rate calibration for *in situ* ^{14}C in quartz, and the excitation functions. We note that these are not entirely independent, as the LSDn-based production rate calibration utilizes both the particle spectra of Sato et al. (2008) and excitation functions of Reedy (2013). Sato et al. (2008) quote statistical uncertainties in their modelled particle fluxes on the order of 5-20% between ca. 10 km altitudes and sea level, respectively, although Lifton et al. (2014) note that predictions within this altitude range show good agreement with measured differential fluxes and no evidence of systematic errors. The conservative uncertainty in the recalibrated *in situ* ^{14}C global production rate in quartz is on the order of 6-7% using the gridded R_{C} geomagnetic framework and LSDn scaling. Reedy (2013) suggests uncertainties on the order of 10% for the empirical excitation functions presented. However, Reedy (2013) also suggests that modelled cross-sections may differ from empirical ones for a given nuclide by a factor of ≈ 2 . Thus, assessing the uncertainty in the modelled functions of JENDL/HE-2007 is more difficult.

We attempted to assess this latter uncertainty by comparing results using JENDL/HE-2007 to predictions incorporating the more recent TENDL-2019 database (Koning et al., 2019). We focused on the proton and neutron excitation functions for ^{14}C production from ^{23}Na , since our predictions using the JENDL/HE-2007 ^{23}Na excitation functions suggest comparable production

to that from O (Fig. 1; Table 2). However, TENDL-2019 excitation functions only extend to an energy of 200 MeV, although at higher resolution than JENDL/HE-2007. We thus compared albite production rates predicted using the JENDL/HE-2007 excitation function alone (Na_J) with those incorporating spliced neutron and proton excitation functions using TENDL-2019 for $E \leq 200$ MeV and JENDL/HE-2007 for $E > 200$ MeV (Na_{TJ}) (Fig. 2).

Neutron and proton excitation functions for ^{23}Na have similar thresholds of ca. 30-35 MeV in both JENDL/HE-2007 and TENDL-2019 (Fig. 2). Of note, the low-energy peaks in the TENDL-2019 excitation functions are narrower, ca. 30% lower, and occur at a slightly higher energy than those of JENDL/HE-2007 (ca. 150 MeV vs. ca. 90 MeV, respectively). However, the predicted production rate for albite using the spliced Na_{TJ} excitation functions is only ca. 3% less than that using the Na_J excitation functions alone (Table 2); also reflected in the lower production proportion from Na of ca. 8% in the spliced version, vs. ca. 13% in Na_J version (Table 3).

Apart from the modelled ^{23}Na excitation functions, the remaining modelled excitation functions have only a minor impact on the overall production rates we predict. The percentages of total production of *in situ* ^{14}C from ^{55}Mn , ^{48}Ti , ^{40}Ca , ^{39}K and ^{31}P range from <0.001% to 0.2% for the compositions considered (Table 3). Even if the modelled reaction cross sections are off by a factor of 2, as suggested from Reedy (2013), the impact to overall production is small. For instance, doubling the percentage of ^{14}C production from Ca for wollastonite would only increase predicted production to 0.4 %. In addition, we argue that calculating production using modelled excitation functions for only the most abundant isotope of each of these elements, instead of excitation functions reflecting their natural isotopic abundances, introduces negligible additional uncertainty. For example, we assume 100% of production of *in situ* ^{14}C from ^{48}Ti , even though ^{48}Ti comprises only 73% of Ti isotopes. However, ^{48}Ti contributes <0.001% of total production for the compositions we considered; it is unlikely that including excitation functions for other common Ti isotopes would change that prediction significantly. Similar arguments can be made for the other isotopes referenced above. We therefore argue that the overall additional uncertainty in our predictions that might be introduced by using more conservative estimates of potential errors in the modelled reaction cross sections would be insignificant relative to other uncertainties in the calculations, for the compositions considered. That said, future additional empirical excitation functions for neutron and proton reactions using these elements in their natural abundances would likely improve our predictions.

Based on these results, we suggest assuming a 10% uncertainty for the JENDL/HE-2007 excitation functions overall, pending empirical validation. Thus, considering the three sources of uncertainty above, we suggest a reasonable estimate of current uncertainty on our theoretical production rates might be on the order of 10-15%, also pending validation with geologic calibrations, assuming extraction and CO_2 purification hurdles can ultimately be overcome.

4.3 Comparisons with previous studies

We compare output of our software framework to two earlier studies that also calculated theoretical *in situ* ^{14}C production rates from targets of varying composition (Fabryka-Martin, 1988; Masarik, 2002), without adjusting our predictions to the geologically calibrated production rate in quartz. First, Fabryka-Martin (1988) estimated SLHL secular equilibrium *in situ* ^{14}C concentrations at depths of ~20 cm for ultramafic rock, basalt, high-Ca granite, low-Ca granite, and limestone compositions, following Parker (1967) (Table 4). The equilibrium concentrations were calculated assuming neutron spallation production only from oxygen and a SLHL production rate of 26 atoms $\text{g}^{-1} \text{y}^{-1}$ from oxygen (Yokoyama et al., 1977) based on excitation functions from Reedy and Arnold (1972). We derived secular equilibrium SLHL production rates from Fabryka-Martin (1988) by multiplying the concentrations by the ^{14}C decay constant of $1.216 \times 10^{-4} \text{y}^{-1}$ (Table 4 – P_{16O-FM}). Considering only theoretical

production from ^{16}O in our results (Total P_{CDpred} in Table 2 multiplied by the corresponding O production proportion in Table 3), our P_{16O} values in Table 4 are ca. 40–45% below those derived from Fabryka-Martin (1988). However, it should be pointed out that Yokoyama et al. (1977) suggest $\pm 35\%$ uncertainty (1σ) on their *in situ* ^{14}C production rate estimate used by Fabryka-Martin (1988), so our theoretical P_{16O} values using more accurate particle fluxes and excitation functions lie well within that range.

The second study we considered (Masarik, 2002) is a conference abstract that presents formulas for estimating compositional dependence of *in situ* cosmogenic nuclide SLHL production rates by neutron spallation, including ^{14}C , derived from numerical simulations. For *in situ* ^{14}C production, Masarik (2002) considers the target elements O, Mg, Al, Si, and Fe, parameterized in terms of weight fractions of each (Table 5). Total production rates from Masarik (2002) (P_{M02}) in Table 5 are typically ca. 10–20% higher than neutron-only theoretical production rates for rock and mineral compositions considered in this study (Neutron P_{CDpred} , Table 2). Being an abstract, details underlying the simulations and calculations in Masarik (2002) are sparse, but we suggest a combination of differences in the differential neutron flux spectra (Masarik and Beer, 1999, vs. Sato et al., 2008) and excitation functions (e.g., Reedy and Masarik, 1995, vs. Reedy, 2013) used in the two studies, as well as unstated uncertainties in the Masarik (2002) coefficients, may be the sources of the discrepancies in the predictions of the respective studies.

We derived a similar elemental parameterization to that of Masarik (2002) for SLHL *in situ* ^{14}C production in atoms $\text{g}^{-1} \text{y}^{-1}$. We include production from both neutrons and protons for each element we consider, given by

$$P_{CDpred} = 29.01[\text{O}] + 15.59[\text{Na}] + 2.19[\text{Mg}] + 1.67[\text{Al}] + 0.84[\text{Si}] + 0.22[\text{P}] + 0.10[\text{Fe}] + 0.08[\text{K}] + 0.06[\text{Ca}] + 0.05[\text{Ti}] + 0.03[\text{Mn}] \quad (4)$$

where the bracketed values are the respective elemental fractions derived from the measured major elemental analysis. *In situ* ^{14}C production rates predicted using this equation for the compositions considered in Table 1 are identical to the P_{CDpred} values in Table 2, since both are derived using the same software framework.

In addition to the theoretical studies, Handwerger et al. (1999) measured *in situ* ^{14}C concentrations in carbonate deposits (limestone bedrock and tufa) from well-preserved Provo-level shoreline features associated with Pleistocene Lake Bonneville, Utah, to calibrate *in situ* ^{14}C spallogenic production rates in calcite. The late Pleistocene lake-level history of Lake Bonneville is well-constrained by traditional radiocarbon dates and has been used for geological calibration of a number of cosmogenic nuclides (Lifton et al., 2015a). *In situ* ^{14}C measurements in Handwerger et al. (1999) were reduced according to standard methods for radiocarbon in organic materials, but Hippe and Lifton (2014) subsequently developed comprehensive data reduction procedures specifically for *in situ* ^{14}C . Unfortunately, Handwerger et al. (1999) do not present full details of their analytical results and calculations – we thus cannot correct their data to current standards using the Hippe and Lifton (2014) protocols. If we assume such corrections would be small relative to the resulting *in situ* ^{14}C concentrations in their calibration samples, neglecting three anomalous results, and using the age of initial Provo shoreline formation from Lifton et al. (2015a) of 18.3 ± 0.3 cal ka BP, their mean *in situ* ^{14}C concentration is $(3.75 \pm 0.26) \times 10^5$ atoms $\text{g}^{-1} \text{CaCO}_3$. This corresponds to a local production rate of ca. 51 atoms $\text{g}^{-1} \text{y}^{-1}$. In contrast, the theoretical local production rate calculated with our software framework is ca. 43.9 atoms $\text{g}^{-1} \text{y}^{-1}$, ~15% lower than the derived local production rate. In addition, the predicted value normalized to P_{Qcal} yields 37.5 atoms $\text{g}^{-1} \text{y}^{-1}$, 27% lower than Handwerger et al. (1999). Given the uncertainties in the uncorrected Handwerger et al. (1999) dataset, and the suggested uncertainties in our method, we find reasonable agreement between our production rate estimates and that of Handwerger et al. (1999).

290 5 Conclusions

As a first step in exploring potential applications of *in situ* ^{14}C to quartz-poor or fine-grained rock types, we have extended the functionality of the MATLAB[®]-based LSDn nuclide-specific scaling framework (Lifton et al., 2014; Lifton, 2016) to estimate spallogenic production of *in situ* ^{14}C in rock and mineral compositions other than pure quartz at sites of interest. We account for compositionally dependent production by using measured and modelled nucleon excitation functions for target elements in major element oxide analyses (e.g., XRF), in concert with secondary cosmic-ray differential fluxes per Lifton et al. (2014). The ratio of resulting theoretical compositionally dependent *in situ* ^{14}C production rates to the corresponding theoretical quartz production rate are then multiplied by the geologically calibrated production rate in quartz, placing the theoretical production rates in a calibrated context. Exploring a broad range of mineral and rock compositions indicates production is dominated by oxygen spallation as expected (>90% at SLHL), but with a general decrease in total production rate with more mafic (particularly Fe-rich) compositions. Although this study confirms previous work identifying Si, Mg, and Al as important targets, we also find for the first time that Na appears to contribute significantly. Future nucleon excitation function measurements, particularly for Na reactions, should improve the robustness of this software tool further. This framework is thus an important initial step forward in applying *in situ* ^{14}C to a broader array of landscapes.

Code availability

305 The MATLAB[®] scripts referenced in this manuscript are available at <https://github.com/nlifton/CD14C> (doi: 10.5281/zenodo.7331947)

Author contributions

The study was conceived by NL and AK. AK and NL developed the MATLAB[®] scripts. Manuscript was written by AK and NL.

Competing interests

310 The authors declare no competing interests.

Acknowledgements

We thank Reto Trappitsch and Irene Schimmelpfennig for their constructive reviews. NL received support from the U.S. National Science Foundation (NSF) award EAR-1560658. AK acknowledges support from a Purdue Research Foundation Ross Fellowship/Assistantship.

315 References

- Balco, G., Stone, J. O., Lifton, N. A. and Dunai, T. J.: A complete and easily accessible means of calculating surface exposure ages or erosion rates from ^{10}Be and ^{26}Al measurements, *Quat. Geochron.*, 3(3), 174–195, doi:10.1016/j.quageo.2007.12.001, 2008.
- Balco, G.: Production rate calculations for cosmic-ray-muon-produced ^{10}Be and ^{26}Al benchmarked against geological calibration data. *Quaternary Geochronology*, 39, 150–173. <https://doi.org/10.1016/j.quageo.2017.02.001>, 2017.

- Barthelmy, D.: Mineralogy Database, <http://www.webmineral.com>, 2014, accessed July 8, 2020
- Bevington P. R. and Robinson D. K.: Data Reduction and Error Analysis for the Physical Sciences. McGraw-Hill, New York, N.Y., 1992
- 325 Borchers, B., Marrero, S., Balco, G., Caffee, M., Goehring, B., Lifton, N., Nishiizumi, K., Phillips, F., Schaefer, J. and Stone, J.: Geological calibration of spallation production rates in the CRONUS-Earth project, *Quat. Geochron.*, 31, 188–198, doi:10.1016/j.quageo.2015.01.009, 2016.
- 330 Brown, D. A., Chadwick, M. B., Capote, R., Kahler, A. C., Trkov, A., Herman, M. W., Sonzogni, A. A., Danon, Y., Carlson, A. D., Dunn, M., Smith, D. L., Hale, G. M., Arbanas, G., Arcilla, R., Bates, C. R., Beck, B., Becker, B., Brown, F., Casperson, R. J., Conlin, J., Cullen, D. E., Descalle, M. A., Firestone, R., Gaines, T., Guber, K. H., Hawari, A. I., Holmes, J., Johnson, T. D., Kawano, T., Kiedrowski, B. C., Koning, A. J., Kopecky, S., Leal, L., Lestone, J. P., Lubitz, C., Márquez Damián, J. I., Mattoon, C. M., McCutchan, E. A., Mughabghab, S., Navratil, P., Neudecker, D., Nobre, G. P. A., Noguere, G., Paris, M., Pigni, M. T., Plompen, A. J., Pritychenko, B., Pronyaev, V. G., Roubtsov, D., Rochman, D., Romano, P., Schillebeeckx, P., Simakov, S., Sin, M., Sirakov, I., Sleaford, B., Sobes, V., Soukhovitskii, E. S., Stetcu, I., Talou, P., Thompson, I., van der Marck, S., Welser-Sherrill, L., Wiarda, D., White, M., Wormald, J. L., Wright, R. Q., Zerkle, M., Žerovnik, G. and Zhu, Y.: ENDF/B-VIII.0: The 8th Major Release of the Nuclear Reaction Data Library with CIELO-project Cross-sections, New Standards and Thermal Scattering Data, *Nucl. Data Sheets*, 148, 1–142, doi:10.1016/j.nds.2018.02.001, 2018.
- 335 Brown, E. T., Trull, T. W., Jean-Baptiste, P., Raisbeck, G., Bourles, D., Yiou, F. and Marty, B.: Determination of cosmogenic production rates of ¹⁰Be, ³He and ³H in water, *Nucl. Instruments Methods Phys. Res. B*, 172, 873–883, 2000.
- 340 Chmeleff, J., von Blanckenburg, F., Kossert, K. and Jakob, D.: Determination of the ¹⁰Be half-life by multicollector ICP-MS and liquid scintillation counting, *Nucl. Inst. Methods Phys. Res. B*, 268(2), 192–199, doi:10.1016/j.nimb.2009.09.012, 2010.
- Cooke, D. J., Humble, J. E., Shea, M. A., Smart, D. F., Lund, N., Rasmussen, I. L., Byrnak, B., Goret, P. and Petrou, N.: On cosmic-ray cut-off terminology, *Nuovo Cim. C*, 14(3), 213–234, doi:10.1007/BF02509357, 1991.
- 345 Fabryka-Martin, J. T.: Production of radionuclides in the earth and their hydrogeologic significance, with emphasis on chlorine-36 and iodine-129. Ph.D. thesis, The University of Arizona., 1988.
- Fukahori, T., Watanabe, Y., Yoshizawa, N., Maekawa, F., Meigo, S. I., Konno, C., Yamano, N., Konobeyev, A. Y. and Chiba, S.: JENDL high energy file, *J. Nucl. Sci. Technol.*, 39, 25–30, doi:10.1080/00223131.2002.10875031, 2002.
- 350 Fülöp, R. H., Fink, D., Yang, B., Codorean, A. T., Smith, A., Wacker, L., Levchenko, V. and Dunai, T. J.: The ANSTO – University of Wollongong in-situ ¹⁴C extraction laboratory, *Nucl. Instruments Methods Phys. Res. Sect. B Beam Interact. With Mater. Atoms*, 438(January 2018), 207–213, doi:10.1016/j.nimb.2018.04.018, 2019.
- Goehring, B. M., Wilson, J. and Nichols, K.: A fully automated system for the extraction of *in situ* cosmogenic carbon-14 in the Tulane University cosmogenic nuclide laboratory, *Nucl. Instruments Methods Phys. Res. Sect. B Beam Interact. With Mater. Atoms*, (December 2017), 1–9, doi:10.1016/j.nimb.2019.02.006, 2019.
- 355 Gosse, J. C. and Phillips, F. M.: Terrestrial *in situ* cosmogenic nuclides: theory and application, *Quat. Sci. Rev.*, 20, 1475–1560, doi:10.1016/S0277-3791(00)00171-2, 2001.
- Grieder, P.: Cosmic Rays at Earth: Researcher’s Reference Manual and Data Book, 1st ed. Elsevier, Amsterdam, 2001.
- Handwerger, D. A., Cerling, T. E. and Bruhn, R. L.: Cosmogenic ¹⁴C in carbonate rocks, *Geomorphology*, 27(March 1998), 1999.
- 360 Heisinger, B., Lal, D., Jull, a. J. T., Kubik, P., Ivy-Ochs, S., Neumaier, S. and Knie, K., Lazarev, V. and Nolte, E.: Production of selected cosmogenic radionuclides by muons 1. Fast muons, *Earth Planet. Sci. Lett.*, 200(3–4), 345–355, doi:10.1016/S0012-821X(02)00640-4, 2002a.
- Heisinger, B., Lal, D., Jull, A. J. T., Kubik, P., Ivy-Ochs, S., Knie, K. and Nolte, E.: Production of selected cosmogenic radionuclides by muons: 2. Capture of negative muons, *Earth Planet. Sci. Lett.*, 200(3–4), 357–369, doi:10.1016/S0012-821X(02)00641-6, 2002b.
- 365 Hippe, K., Jansen, J. D., Skov, D. S., Lupker, M., Ivy-Ochs, S., Kober, F., Zeilinger, G., Capriles, J. M., Christl, M., Maden, C., Vockenhuber, C. and Egholm, D. L.: Cosmogenic *in situ* ¹⁴C-¹⁰Be reveals abrupt Late Holocene soil loss in the Andean Altiplano, *Nat. Commun.*, 12, 1–9, doi:10.1038/s41467-021-22825-6, 2021.
- Hippe, K.: Constraining processes of landscape change with combined *in situ* cosmogenic ¹⁴C-¹⁰Be analysis, *Quat. Sci. Rev.*, 173, 1–19, doi:10.1016/j.quascirev.2017.07.020, 2017.

- 370 Hippe, K., Kober, F., Wacker, L., Fahrni, S. M., Ivy-Ochs, S., Akçar, N., Schlüchter, C. and Wieler, R.: An update on *in situ* cosmogenic ^{14}C analysis at ETH Zürich, Nucl. Instruments Methods Phys. Res. Sect. B Beam Interact. With Mater. Atoms, 294, 81–86, doi:10.1016/j.nimb.2012.06.020, 2013.
- Hippe, K. and Lifton, N. A.: Calculating isotope ratios and nuclide concentrations for *in situ* cosmogenic ^{14}C analyses. Radiocarb., 56(3), 1167–1174. <https://doi.org/10.2458/56.17917>, 2014.
- 375 Imamura, M., Nagai, H., Takabatake, M., Shibata, S., Kobayashi, K., Yoshida, K., Ohashi, H., Uwamino, Y. and Nakamura, T.: Measurements of production cross sections of C and ^{26}Al with high-energy neutrons up to $E_n = 38$ MeV by accelerator mass spectrometry, Nucl. Inst. Methods Phys. Res. B, 52(3–4), 595–600, doi:10.1016/0168-583X(90)90482-A, 1990.
- Jull, A. J. T., Cloutd, S., Donahue, D. J., Sisterson, J. M., Reedy, R. C. and Masarik, J.: ^{14}C depth profiles in Apollo 15 and 17 cores and lunar rock 68815, Geochim. Cosmochim. Acta, 62(17), 3025–3036, doi:10.1016/S0016-7037(98)00193-8, 1998.
- 380 Jull, A. J. T., Lifton, N., Phillips, W., & Quade, J.: Studies of the production rate of cosmic-ray produced ^{14}C in rock surfaces. Nucl. Inst. Methods Phys. Res. B 92, 308–310, 1994.
- Jull, A.T.J., Wilson, A.E., Donahue, D.J., Toolin, L.J., Burr, G.S.: Measurements of cosmogenic ^{14}C produced by spallation in high- altitude rocks. Radiocarbon 34, 737-744, 1992.
- Jull, A. J. T., Donahue, D. J. and Linick, T. W.: Carbon-14 activities in recently fallen meteorites and Antarctic meteorites, 385 Geochim. Cosmochim. Acta, 53(8), 2095–2100, doi:10.1016/0016-7037(89)90327-X, 1989.
- Koning, A. J., Rochman, D., Sublet, J., Dzysiuk, N., Fleming, M. and Van Der Marck, S.: TENDL : Complete Nuclear Data Library for Innovative Nuclear Science and Technology, Nucl. Data Sheets, 155, 1–55, doi:10.1016/j.nds.2019.01.002, 2019.
- Korschinek, G., Bergmaier, A., Faestermann, T., Gerstmann, U. C., Knie, K., Rugel, G., Wallner, A., Dillmann, I., Dollinger, G., 390 Lierse von Gostomski, C., Kossert, K., Maiti, M., Poutivtsev, M. and Remmert, A.: A new value for the half-life of ^{10}Be by Heavy-Ion Elastic Recoil Detection and liquid scintillation counting, Nucl. Inst. Methods Phys. Res. B, 268(2), 187–191, doi:10.1016/j.nimb.2009.09.020, 2010.
- Lifton, N., Caffee, M., Finkel, R., Marrero, S., Nishiizumi, K., Phillips, F.M., Goehring, B., Gosse, J., Stone, J., Schaefer, J., Theriault, B., Jull, A.J.T., Fifield, K.: *In situ* cosmogenic nuclide production rate calibration for the CRONUS-Earth project 395 from Lake Bonneville, Utah, shoreline features. Quat. Geochron. 26, 55-69. Doi:10.1016/j.quageo.2014.11.002, 2015a.
- Lifton, N., Goehring, B., Wilson, J., Kubley, T. and Caffee, M.: Progress in automated extraction and purification of *in situ* ^{14}C from quartz: Results from the Purdue *in situ* ^{14}C laboratory, Nucl. Instruments Methods Phys. Res. Sect. B Beam Interact. With Mater. Atoms, 361, 381–386, doi:10.1016/j.nimb.2015.03.028, 2015b.
- Lifton, N., Sato, T. and Dunai, T. J.: Scaling *in situ* cosmogenic nuclide production rates using analytical approximations to 400 atmospheric cosmic-ray fluxes, Earth Planet. Sci. Lett., 386, 149–160, doi:10.1016/j.epsl.2013.10.052, 2014.
- Lifton, N. A., Smart, D. F. and Shea, M. A.: Scaling time-integrated *in situ* cosmogenic nuclide production rates using a continuous geomagnetic model, Earth Planet. Sci. Lett., 268, 190–201, doi:10.1016/j.epsl.2008.01.021, 2008.
- Lifton, N., Jull, A. J. T. and Quade, J.: A new extraction technique and production rate estimate for *in situ* cosmogenic ^{14}C in quartz, Geochim. Cosmochim. Acta, 65(12), 1953–1969, doi:10.1016/S0016-7037(01)00566-X, 2001.
- 405 Lifton N. A.: A new extraction technique and production rate estimate for *in situ* cosmogenic ^{14}C in quartz. Ph.D. Dissertation, University of Arizona, 1997.
- Lupker, M., Hippe, K., Wacker, L., Steinemann, O., Tikhomirov, D., Maden, C., Haghipour, N. and Synal, H. A.: In-situ cosmogenic ^{14}C analysis at ETH Zürich: Characterization and performance of a new extraction system, Nucl. Instruments Methods Phys. Res. Sect. B Beam Interact. With Mater. Atoms, 457(March), 30–36, doi:10.1016/j.nimb.2019.07.028, 2019.
- 410 Lupker, M., Hippe, K., Wacker, L., Kober, F., Maden, C., Braucher, R., Bourlès, D., Romani, J. R. V. and Wieler, R.: Depth-dependence of the production rate of *in situ* ^{14}C in quartz from the Leymon High core, Spain, Quat. Geochron., 28, 80–87, doi:10.1016/j.quageo.2015.04.004, 2015.
- Marrero, S.M., Phillips, F.M., Caffee, M.W., and Gosse, J.C.: CRONUS-Earth cosmogenic ^{36}Cl calibration: Quat. Geochron. 31, 199–219, doi:10.1016/j.quageo.2015.10.002, 2016a.
- 415 Marrero, S. M., Phillips, F. M., Borchers, B., Lifton, N., Aumer, R. and Balco, G.: Cosmogenic nuclide systematics and the CRONUScalc program, Quat. Geochron., 31, 160–187, doi:10.1016/j.quageo.2015.09.005, 2016b.
- Masarik, J. and Beer, J.: An updated simulation of particle fluxes and cosmogenic nuclide production in the Earth’s atmosphere, J. Geophys. Res., 114, 1–9, doi:10.1029/2008JD010557, 2009.

- Masarik, J.: Numerical simulation of in-situ production of cosmogenic nuclides, *Geochim. Cosmochim. Acta* 66, Suppl. 1, A491, 2002.
- Masarik, J. and Reedy, R. C.: Monte Carlo simulations of in-situ-produced cosmogenic nuclides, in *Santa Fe Workshop on Secular Variations*, 163–164., 1995.
- Martin, L. C. P., Blard, P. H., Balco, G., Lavé, J., Delunel, R., Lifton, N. and Laurent, V.: The CREP program and the ICE-D production rate calibration database: A fully parameterizable and updated online tool to compute cosmic-ray exposure ages, *Quat. Geochron.*, 38, 25–49, doi:10.1016/j.quageo.2016.11.006, 2017.
- Michel, R., Gloris, M., Lange, H.-J., Leya, I., Lupke, M., Herpers, U., Dittrich-Hannen, B., Rosel, R., Schiek, T., Filges, D., Dragovitsch, P., Sutter, M., Hofmann, H.-J., Wolfig, W., Kubik, P. W., Baur, H. and Wieler, R.: Nuclide production by proton-induced reactions on elements ($6 < Z < 29$) in the energy range from 800 to 2600 MeV, *Nucl. Instr. Methods Phys. Res. B*, 103, 183–222, 1995.
- Morimoto, N.: Nomenclature of pyroxenes. *Mineralogy and Petrology*, 39(1), 55–76. <https://doi.org/10.1007/bf01226262>, 1988.
- Nishiizumi, K.: Preparation of ^{26}Al AMS standards. *Nuclear. Instr. Meth. Phys. Res. B*, 223, 388–392, doi:10.1016/j.nimb.2004.04.075, 2004.
- Nishiizumi, K., Finkel, R.C., Klein, J., Kohl, C.P.: Cosmogenic production of ^7Be and ^{10}Be in water targets. *Journal of Geophysical Research* 101, 22,225–22,232, 1996.
- Parker, R. L.: Data of Geochemistry, U. S. Geol. Surv. Prof. Paper 440-D, ed. M. Fleischer, 19 p., 1967.
- Pavón-Carrasco, F.J., Osete, M.L., Torta, J.M., De Santis, A.: A geomagnetic field model for the Holocene based on archaeomagnetic and lava flow data. *Earth Planet. Sci. Lett.* 388, 98–109, 2014.
- Reedy, R. C.: Cosmogenic-nuclide production rates: Reaction cross section update, *Nucl. Instr. Meth. Phys. Res. B*, 294, 470–474, doi:10.1016/j.nimb.2011.08.034, 2013.
- Reedy, R. C.: Proton cross-sections for producing cosmogenic radionuclides, *Lunar Planet. Sci* 38, 1329–1330, 2007.
- Reedy, R.C.: A model for GCR-particle fluxes in stony meteorites and production rates of cosmogenic nuclides: *Journal of Geophys. Res.* 90, Suppl., C722–C728, doi:10.1029/jb090is02p0c722, 1985.
- Sato, T. and Niita, K.: Analytical functions to predict cosmic-ray neutron spectra in the atmosphere, *Radiat. Res.*, 166(3), 544–555, doi:10.1667/RR0610.1, 2006.
- Sato, T., Yasuda, H., Niita, K., Endo, A., Sihver, L., Sato, T., Yasuda, H., Niita, K., Endo, A. and Sihver, L.: Development of PARMA: PHITS-Based Analytical Radiation Model in the Atmosphere, *Radiat. Res.*, 170(2), 244–259, 2008.
- Schimmelpfennig, I., Schaefer, J. M., Goehring, B. M., Lifton, N., Putnam, A. E. and Barrell, D. J. A.: Calibration of the *in situ* cosmogenic ^{14}C production rate in New Zealand’s Southern Alps, *J. Quat. Sci.*, 27, 671–674, doi:10.1002/jqs.2566, 2012.
- Sisterson, J. M., Schneider, R. J. I., Jull, A. J. T., Donahue, D. J., Cloudt, S., Kim, K., Beverding, A., Englert, P. A. J., Castaneda, C., Vincent, J. and Reedy, R. C.: Revised solar cosmic ray fluxes estimated using measured depth profiles of ^{14}C in Lunar rocks; The importance of good ^{14}C cross section determinations, *Lunar Planet. Sci.* 22, 1996.
- Sisterson, J., Jull, A. J. T., Beverding, A., Koehler, A. M., Castaneda, C., Vincent, J., Donahue, D. J., Englert, P. A. J., Gans, C., Young, J. and Reedy, R. C.: Proton production cross-sections for ^{14}C from silicon and oxygen: implications for cosmic-ray studies, *Nucl. Instruments Methods Phys. Res. B*, 92, 510–512, 1994.
- Thomas, J. H., Rau, R. L., Skelton, R. T. and Kavanagh, R. W.: Half-life of ^{26}Al , *Phys. Rev. C*, 30(1), 385–387, 1984.
- Vermeesch, P., Baur, H., Heber, V. S., Kober, F., Oberholzer, P., Schaefer, J. M., Schlüchter, C., Strasky, S. and Wieler, R.: Cosmogenic ^3He and ^{21}Ne measured in targets after one year of exposure in the Swiss Alps, *Earth Planet. Sci. Lett.*, 284(3–4), 417–425, doi:10.1016/j.epsl.2009.05.007, 2009.
- Von Blanckenburg, F.: The control mechanisms of erosion and weathering at basin scale from cosmogenic nuclides in river sediment, *Earth Planet. Sci. Lett.*, 237(3–4), 462–479, doi:10.1016/j.epsl.2005.06.030, 2005.
- Watanabe, Y., Kosako, K., Kunieda, S., Chiba, S., Fujimoto, R., Harada, H., Kawai, M., Maekawa, F., Murata, T., Nakashima, H., Niita, K., Shigyo, N., Shimakawa, S., Yamano, N. and Fukahori, T.: Status of JENDL high energy file, *J. Korean Phys. Soc.*, 59(23), 1040–1045, doi:10.3938/jkps.59.1040, 2011.
- Wright, T., Bennett, S., Heinitz, S., Köster, U., Mills, R., Soldner, T., Steier, P., Wallner, A., and Wieninger, T.: Measurement of the $^{13}\text{C}(n,\gamma)$ thermal cross section via neutron irradiation and AMS, *Eur. Phys. J. A*, 55, 200, doi:10.1140/epja/i2019-12893-0, 2019.

Yokoyama, Y., Reyss, J. L. and Guichard, F.: Production of radionuclides by cosmic rays at mountain altitudes, *Earth Planet. Sci. Lett.*, 36(1), 44–50, doi:10.1016/0012-821X(77)90186-8, 1977.

470 Young, N. E., Schaefer, J. M., Goehring, B., Lifton, N., Schimmelpfennig, I. and Briner, J. P.: West Greenland and global *in situ* ^{14}C production-rate calibrations, *J. Quat. Sci.*, 29(5), 401–406, doi:10.1002/jqs.2717, 2014.

Figures

475 **Figure 1:** Measured (Reedy, 2013) (top panels) and modelled (bottom panels) neutron and proton reaction excitation functions for *in situ* ^{14}C production from various targets. The lines are linearly interpolated between points. Note that modelled predictions for ^{23}Na (JENDL/HE-2007; Fukahorita et al., 2002; Watanabe et al., 2011) suggest the highest production of all nuclides considered.

480 **Figure 2:** Modelled neutron (top) and proton (bottom) cross-sections for ^{23}Na from JENDL/HE-2007 (Na_J , solid line) compared to the spliced TENDL-2019 at energies ≤ 0.2 GeV and JENDL/HE-2007 > 0.2 GeV ($^{23}\text{Na}_{TJ}$, dashed line). Differential neutron and proton fluxes at SLHL (J_N and J_P , respectively) (Sato et al., 2008) are plotted in their respective panes to illustrate the combined effect of excitation function and flux on *in situ* ^{14}C production.

485 **Figure 3:** Predicted theoretical SLHL production of *in situ* ^{14}C (P_{CDpred}) in minerals (left) and rocks (right) relative to that in pure quartz (dashed grey line). The color of each symbol reflects the element that contributes the highest proportion of production after oxygen and silica.

Tables

490 **Table 1:** Elemental oxide compositions (weight %) for selected silicate minerals (Barthelmy, 2014; Morimoto, 1988) and rock types (Parker, 1967), used to calculate number densities (Eq. 2).

Table 2: Predicted modern *in situ* ^{14}C spallogenic production rates (atoms $\text{g}^{-1} \text{y}^{-1}$) at SLHL from neutrons and protons in minerals and rock types considered, both theoretical (P_{CDpred}) and normalized to calibrated production in quartz (P_{CD}) using the gridded R_C record of Lifton (2016).

Table 3: Percentage of total theoretical predicted modern SLHL *in situ* ^{14}C production (P_{CDpred}) by element for each mineral and rock type considered.

500 **Table 4:** Predicted modern *in situ* ^{14}C production rates at SLHL for neutron spallation from ^{16}O derived from secular equilibrium concentrations (N_{SE}) at ca. 20-cm depth for different rock types (Fabryka-Martin, 1988) compared to our software framework. Note that these estimates are not normalized relative to P_{Qcal} , for straightforward comparison to Fabryka-Martin's (1988) predictions.

505 **Table 5:** Neutron-only SLHL *in situ* ^{14}C production based on Masarik (2002; P_{M02}) theoretical predictions for compositions considered in this work, compared to modern SLHL neutron-only production predicted here (also see Table 2). Note that these estimates are not normalized relative to P_{Qcal} , to enable direct comparison to Masarik's (2002) predictions.

Table 1:

Mineral	Composition	SiO ₂	TiO ₂	Al ₂ O ₃	FeO	Fe ₂ O ₃	MnO	MgO	CaO	Na ₂ O	K ₂ O	P ₂ O ₅	LOI ²
<i>Quartz</i>	SiO ₂	100	-	-	-	-	-	-	-	-	-	-	-
<i>Albite</i>	NaAlSi ₃ O ₈	68.74	-	19.44	-	-	-	-	-	11.82	-	-	-
<i>Anorthite</i>	CaAl ₂ Si ₂ O ₈	43.19	-	36.65	-	-	-	-	20.16	-	-	-	-
<i>Orthoclase</i>	KAlSi ₃ O ₈	64.76	-	18.32	-	-	-	-	-	-	16.92	-	-
<i>Forsterite</i>	Mg ₂ SiO ₄	42.71	-	-	-	-	-	57.30	-	-	-	-	-
<i>Fayalite</i>	Fe ₂ SiO ₄	29.49	-	-	70.52	-	-	-	-	-	-	-	-
<i>Wollastonite</i>	Ca ₂ Si ₂ O ₆	51.73	-	-	-	-	-	-	48.28	-	-	-	-
<i>Augite</i> ¹	(Ca,Mg,Fe)(Mg,Fe)Si ₂ O ₆	24.18	-	-	16.83	-	-	7.32	10.35	-	-	-	-
<i>Ferrosilite</i>	Fe ₂ Si ₂ O ₆	45.54	-	-	54.46	-	-	-	-	-	-	-	-
<i>Enstatite</i>	Mg ₂ Si ₂ O ₆	59.85	-	-	-	-	-	40.15	-	-	-	-	-
<i>Calcite</i> ²	CaCO ₃	-	-	-	-	-	-	-	56.03	-	-	-	43.97
<i>Dolomite</i> ²	CaMg(CO ₃) ₂	-	-	-	-	-	-	21.86	30.41	-	-	-	47.73
Rock type³													
<i>Ultramafic</i>	—	40.64	0.05	0.66	-	14.09	0.19	42.94	0.98	0.77	0.04	0.04	-
<i>Basalt</i>	—	51.34	1.50	16.55	-	12.24	0.26	7.46	9.40	2.62	1.00	0.32	-
<i>Hi-Ca Granite</i>	—	67.16	0.57	15.49	-	4.23	0.07	1.56	3.54	3.83	3.04	0.21	-
<i>Low-Ca Granite</i>	—	74.22	0.20	13.60	-	2.03	0.05	0.27	0.71	3.48	5.06	0.14	-
<i>Granodiorite</i>	—	69.09	0.57	14.55	-	3.86	0.08	0.93	2.21	3.73	4.02	0.16	-

¹ Assumed empirical composition of augite (Morimoto, 1988; <https://www.mindat.org/min-419.html>):
(Ca_{0.6}Mg_{0.2}Fe_{0.2})(Mg_{0.5}Fe_{0.5})Si₂O₆

² LOI = Loss on ignition. Used in oxygen number density calculation for carbonates; assumed to be entirely CO₂ in those cases.

515 ³ Compositions from Parker (1967)

Table 2

Mineral	<i>Neutron P_{CDpred} at $g^{-1} y^{-1}$</i>	<i>Proton P_{CDpred} at $g^{-1} y^{-1}$</i>	<i>Total P_{CDpred} at $g^{-1} y^{-1}$</i>	<i>P_{CD} at $g^{-1} y^{-1}$</i>	<i>% Diff P_{CD} vs. P_{Qcal}</i>
<i>Quartz</i>	15.37	0.47	15.84	13.50	0.0
<i>Albite</i>	15.49	0.48	15.97	13.61	0.8
<i>Albite¹</i>	14.95	0.48	15.43	13.15	-2.6
<i>Anorthite</i>	13.43	0.42	13.85	11.80	-12.6
<i>Orthoclase</i>	13.20	0.39	13.60	11.59	-14.2
<i>Forsterite</i>	13.67	0.46	14.12	12.03	-10.9
<i>Fayalite</i>	9.01	0.27	9.28	7.91	-41.4
<i>Wollastonite</i>	11.85	0.36	12.21	10.41	-22.9
<i>Augite</i>	12.00	0.37	12.38	10.54	-21.9
<i>Ferrosilite</i>	10.46	0.32	10.78	9.18	-32.0
<i>Enstatite</i>	14.18	0.46	14.64	12.47	-7.6
<i>Calcite</i>	13.55	0.38	13.94	11.88	-12.0
<i>Dolomite</i>	14.96	0.44	15.40	13.12	-2.8
Rock					
<i>Ultramafic</i>	13.11	0.43	13.54	11.54	-14.5
<i>Basalt</i>	13.72	0.43	14.15	12.06	-10.7
<i>Hi-Ca Granite</i>	14.30	0.44	14.75	12.57	-6.9
<i>Low-Ca Granite</i>	14.52	0.45	14.97	12.76	-5.5
<i>Granodiorite</i>	14.27	0.44	14.71	12.54	-7.1

¹Production is calculated using the spliced TENDL-2019 and JENDL/HE-2007 proton and neutron excitation functions (Na_{TJ} in text). All other Na production rates use JENDL/HE-2007 exclusively.

Table 3

	O	Si	Ti	Al	Fe²⁺	Fe³⁺	Mn	Mg	Ca	Na	K	P
Minerals												
<i>Quartz</i>	97.5	2.5	-	-	-	-	-	-	-	-	-	-
<i>Albite</i>	88.67	1.70	-	1.08	-	-	-	-	-	8.56	-	-
<i>Albite¹</i>	88.62	1.36	-	1.72	-	-	-	-	-	8.30	-	-
<i>Anorthite</i>	96.37	1.23	-	2.33	-	-	-	-	0.07	-	<0.01	-
<i>Orthoclase</i>	98.11	0.63	-	1.19	-	-	-	-	-	-	0.08	-
<i>Forsterite</i>	93.45	1.19	-	-	-	-	-	5.36	-	-	-	-
<i>Fayalite</i>	98.14	1.25	-	-	0.61	-	-	-	-	-	-	-
<i>Wollastonite</i>	98.16	1.67	-	-	-	-	-	-	0.17	-	-	-
<i>Augite</i>	96.87	1.65	-	-	0.14	-	-	1.30	0.05	-	-	-
<i>Ferrosilite</i>	97.93	1.66	-	-	0.41	-	-	-	-	-	-	-
<i>Enstatite</i>	94.77	1.61	-	-	-	-	-	3.62	-	-	-	-
<i>Calcite</i>	99.82	-	-	-	-	-	-	-	0.18	-	-	-
<i>Dolomite</i>	98.04	-	-	-	-	-	-	1.87	0.09	-	-	-
Rock type												
<i>Ultramafic</i>	93.84	1.18	<0.01	0.04	<0.01	0.08	<0.01	4.20	<0.01	0.66	<0.01	<0.01
<i>Basalt</i>	94.60	1.43	<0.01	1.08	<0.01	0.07	<0.01	0.70	0.03	2.14	<0.01	<0.01
<i>Hi-Ca Granite</i>	94.09	1.79	<0.01	1.01	<0.01	0.02	<0.01	0.14	0.01	3.00	0.01	<0.01
<i>Low-Ca Granite</i>	94.50	1.95	<0.01	0.89	<0.01	0.01	<0.01	0.02	<0.01	2.69	0.02	<0.01
<i>Granodiorite</i>	94.22	1.85	<0.01	0.95	<0.01	0.02	<0.01	0.08	0.01	2.93	0.02	<0.01

530 ¹PProduction is calculated using the spliced TENDL-2019 and JENDL/HE-2007 proton and neutron excitation functions (Na_{TJ} in text). All other Na production rates use JENDL/HE-2007 exclusively.

Table 4

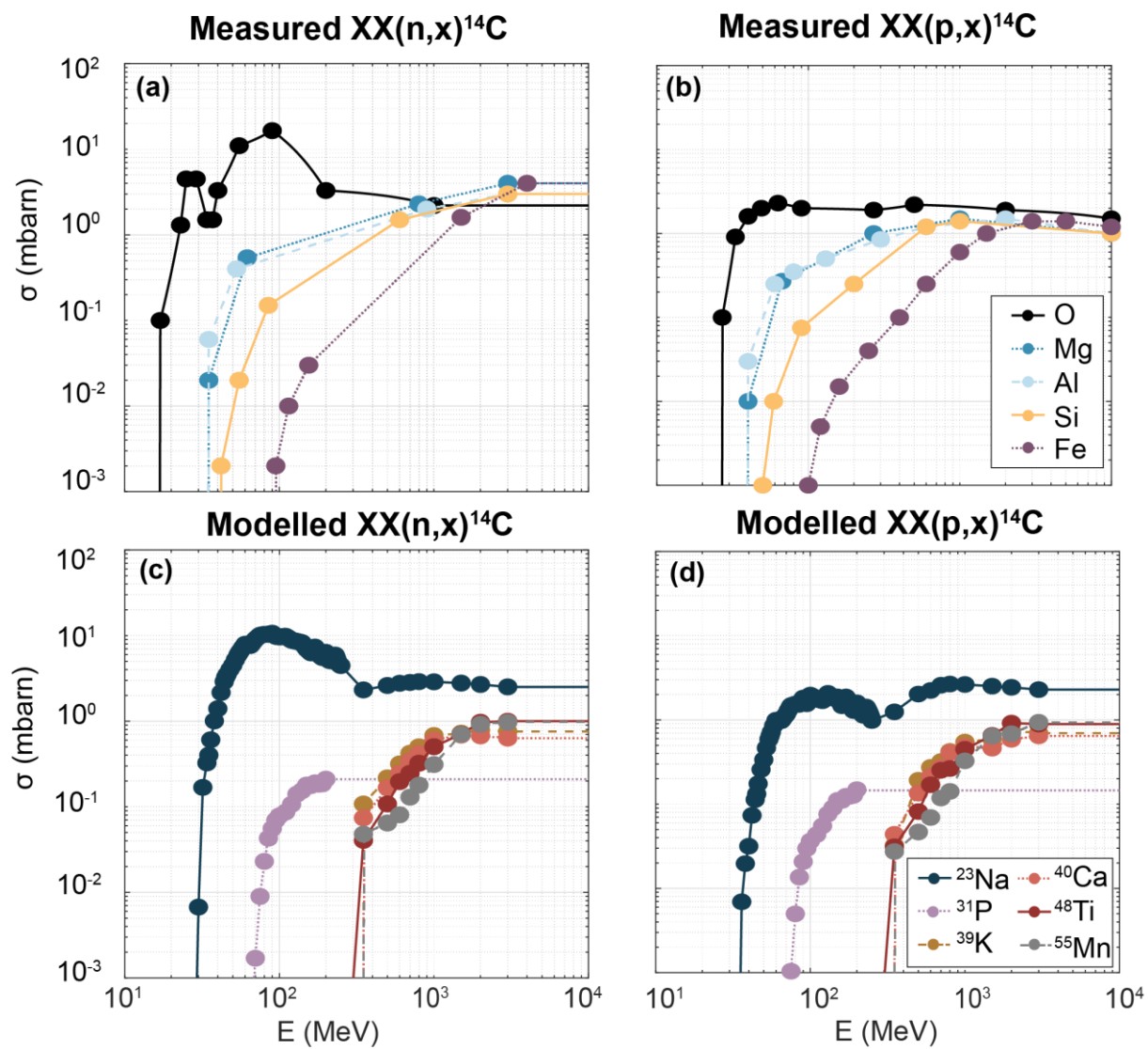
Rock Type	Depth (m)¹	density	N_{SE} (at g⁻¹)¹	P_{160-FM}^1 (at g⁻¹y⁻¹)	P_{160}^2 (at g⁻¹y⁻¹)
<i>Ultramafic</i>	0.18		135706	16.4	9.0
<i>Basalt</i>	0.18		132621	16.0	9.3
<i>Hi-Ca Granite</i>	0.19		148043	17.9	9.7
<i>Low-Ca Granite</i>	0.19		151127	18.3	9.9
<i>Limestone</i>	0.19		151127	18.3	10.1

¹Data from Fabryka-Martin (1988), assumes SLHL production rate from oxygen in Yokoyama et al. (1977)
²Data from this study assuming only production from neutron spallation of O and an attenuation length of 160 g cm⁻²

Table 5

Mineral	P_{M02} (at g⁻¹ y⁻¹)	P_{CDn} (at g⁻¹ y⁻¹)
<i>Quartz</i>	18.72	15.37
<i>Albite</i>	17.20	15.49
<i>Anorthite</i>	16.25	13.43
<i>Orthoclase</i>	16.20	13.20
<i>Forsterite</i>	16.43	13.67
<i>Fayalite</i>	11.06	9.01
<i>Wollastonite</i>	14.42	11.85
<i>Augite</i>	14.59	12.00
<i>Ferrosilite</i>	12.80	10.46
<i>Enstatite</i>	17.11	14.18
<i>Calcite</i>	16.48	13.55
<i>Dolomite</i>	18.12	14.96
Rock		
<i>Ultramafic</i>	15.27	13.11
<i>Basalt</i>	15.38	13.72
<i>Hi-Ca Granite</i>	17.15	14.30
<i>Low-Ca Granite</i>	17.15	14.52
<i>Granodiorite</i>	17.14	14.27

Figure 1



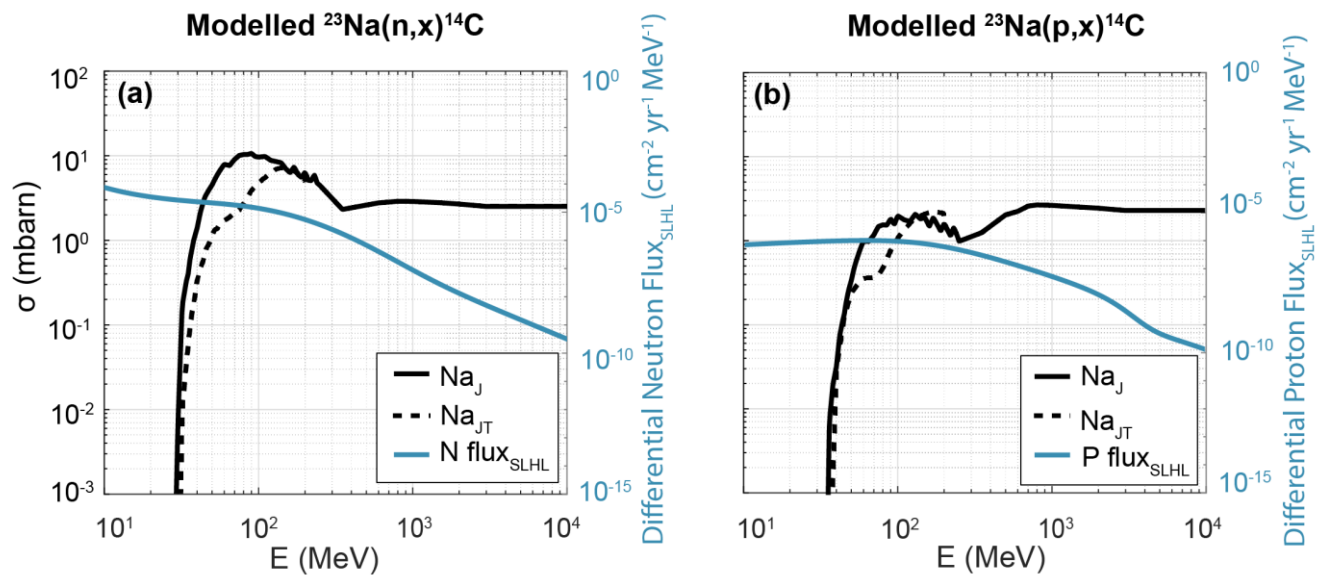


Figure 3

